Title
Reconfigurable microfluidic pump enabled by opto-electrical-thermal transduction

Journal
Applied Physics Letters, 103(17)

ISSN
0003-6951

Authors
Takeuchi, Masaru
Hagiwara, Masaya
Haulot, Gauvain
et al.

Publication Date
2013-10-21

DOI
10.1063/1.4824989

Peer reviewed

Reconfigurable microfluidic pump enabled by opto-electrical-thermal transduction

Masaru Takeuchi, Masaya Hagiwara, Gauvain Haulot, and Chih-Ming Ho

Citation: Appl. Phys. Lett. **103**, 174101 (2013); doi: 10.1063/1.4824989
View online: http://dx.doi.org/10.1063/1.4824989
View Table of Contents: http://apl.aip.org/resource/1/APPLAB/v103/i17
Published by the AIP Publishing LLC.

Reconfigurable microfluidic pump enabled by opto-electrical-thermal transduction

Masaru Takeuchi,[1,2] Masaya Hagiwara,[1] Gauvain Haulot,[1] and Chih-Ming Ho[1]
[1]*Department of Mechanical and Aerospace Engineering, University of California, Los Angeles, Los Angeles 90095, USA*
[2]*Department of Micro-Nano Systems Engineering, Nagoya University, Aichi 464-8603, Japan*

(Received 24 June 2013; accepted 30 July 2013; published online 21 October 2013)

Flexible integration of a microfluidic system comprising pumps, valves, and microchannels was realized by an optoelectronic reconfigurable microchannels (OERM) technique. Projecting a low light fluidic device pattern—e.g., pumps, valves, and channels—onto an OERM platform generates Joule heating and melts the substrate in the bright area on the platform; thus, the fluidic system can be reconfigured by changing the projected light pattern. Hexadecane was used as the substrate of the microfluidic system. The volume change of hexadecane during the liquid–solid phase transition was utilized to generate pumping pressure. The system can pump nanoliters of water within several seconds. © *2013 AIP Publishing LLC*. [http://dx.doi.org/10.1063/1.4824989]

Microfluidic circuitry can conduct, transport, and mix fluids in small volumes for chemical reaction analysis, biomarker detection, and microorganism manipulation.[1–4] Pumps and valves are necessary actuators to move or stop fluids in microchannel networks. Peristaltic pumps in a silicon substrate[5] or polydimethylpolysiloxane (PDMS) substrate[6] have been demonstrated for integrated microfluidic systems. However, once the devices are made, relocation and reconnection are not possible. External conventional syringe pumps and macro mechanical valves are commonly used to interface with microchannels despite the inconvenience. When multiple external pumps and valves are used, the system is bulky and has large dead volumes, which defeats the purpose of using microfluidics.

Actuators such as pumps and valves have moving parts and need power to drive them. Micro pumps can be actuated by magnetic force,[7] optical power,[8,9] electrorheological (ER) fluid,[10] capillary force,[11] electrokinetics,[12] and piezoelectric devices.[13] Those devices make it difficult to control the pumping volume,[11] multiple pumps, and valves independently at the same time.[7,10,12,13] Some devices require a high power source such as a laser[8,9] or high-voltage source[10] for actuation.

A recent innovative idea of applying optoelectronic effects such as optoelectronic tweezers[14,15] and optoelectrowetting[16] was successfully developed to move large numbers of particles or liquid droplets in parallel. These optoelectronic actuators use hydrogenated amorphous silicon (a-Si:H) as a photoconductive substrate. a-Si:H was developed mainly for solar cell applications[17] because amorphous silicon absorbs much more light than crystalline silicon. A low-intensity light beam can draw a pattern on the surface and form a reconfigurable "low impedance electrode" for electrical current to flow through. Electrokinetic force can then be generated by these reconfigurable electrodes to manipulate particles using a-Si:H.

By projecting a low-power light emitting diode (LED) light pattern onto a-Si:H, we applied the optoelectronic concept[14] and were able to transduce the low-power optical energy into high-power thermal energy through electrical heating. The heat was high enough to melt substrate materials such as frozen hexadecane.[18] The melting–freezing process by an on–off light pattern can be used as to form an optoelectronic reconfigurable microchannels (OERM) platform.[18] A single low-intensity light source can project intricate patterns onto the substrate to form a reconfigurable fluidic network. However, only microchannels were fabricated; the actuators were still syringe pumps and macro mechanical valves,[18,19] which limit the potential of OERM.

We utilized the volume change of the substrate material during the liquid–solid phase transition on the OERM platform to form a pump. We further demonstrated that a phase transition–based pump can be formed in only a few seconds and provide sufficient hydrodynamic pressure. Figure 1 shows the concept of fabricating the pump, valve, and microchannel using the OERM technique. The OERM platform is placed on a transparent cooler to keep the working medium frozen. The OERM has three layers of patterned coatings on a glass substrate: indium tin oxide (ITO), a-Si:H, and gold, as shown in Fig. 1. A voltage bias is applied between the ITO and gold layer. The projected light absorbed by the photoconductive layer (a-Si:H) generates a low-impedance pattern that allows current to flow across the layer. The currents generate local Joule heating, which is transferred to the frozen material. Hence, the frozen liquid on the platform is melted according to the light. The melted region can be frozen again when the light pattern is turned off.

Pumps, valves, and channels can be formed by melting or freezing the working material on the a-Si:H substrate at any desired instant and location. The pumping function relies on the volume change during the solid–liquid phase transition of working media in the substrate. During the phase transition of hexadecane, the solid volume is 88% of the liquid volume. This volume change produces the pumping pressure gradient in the microchannel. In the case of solidification after the light pattern has been turned off, low pressure is produced at the pump–channel connection. Consequently, fluid in the channel is sucked toward the pump (Fig. 1(i)). On the other hand, when the light patterns are turned on, the working medium starts to melt and its volume increases. Then, higher pressure can be generated, and

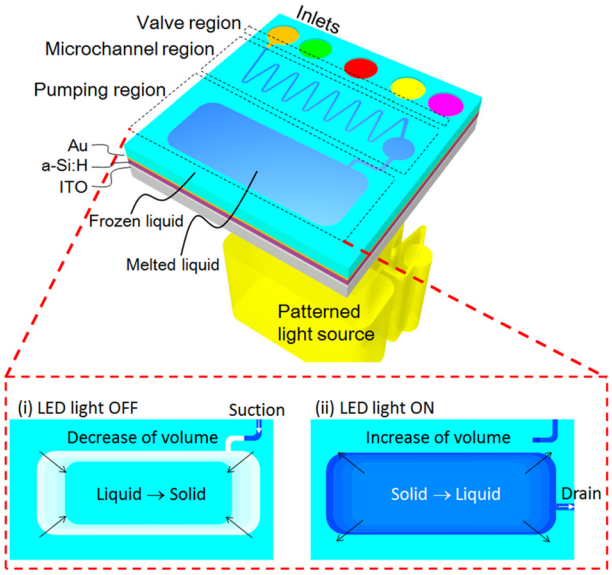

FIG. 1. Concept of reconfigurable microfluidic pump using optoelectronic heating.

fluid moves out from the pump area into the channel (Fig. 1(ii)). A single low-power light source can be used to actuate the multiple pumps and valves simultaneously as well as reconfigure the microchannels when the OERM platform is used.

The phase transition temperature of the OERM working medium of hexadecane ($C_{16}H_{34}$) is not a fixed temperature and occurs in the temperature range of 16–18 °C.[20,21] This melting temperature range is suitable for operation at room temperature. In addition, hexadecane has a low latent heat (184 kJ/L) compared to water (332 kJ/L). As a result, hexadecane can be frozen or melted within a short time.

The melting and freezing time durations of hexadecane determine the time constant of the pump. The dimensions on the x–y plane are much larger than that in the z direction. Therefore, the one-dimensional (1D) unsteady heat conduction equation should be a reasonable model for studying the characteristics of the pump

$$\frac{\partial T(z,t)}{\partial t} = D \times \frac{\partial^2 T(z,t)}{\partial z^2} + q. \quad (1)$$

$T(z,t)$ is the temperature at position z and time t, D is the thermal diffusivity, and q is the heat generation. From Eq. (1), the differential equation can be written as

$$\frac{T(z,t+\Delta t) - T(z,t)}{\Delta t} = D \times \frac{T(z+\Delta z,t) - 2T(z,t) + T(z-\Delta z,t)}{(\Delta z)^2} + q. \quad (2)$$

The temperature $T(z,t+\Delta t)$ can be calculated from the three temperatures at the last time step $T(z+\Delta z,t)$, $T(z,t)$, and $T(z\text{-}\Delta z,t)$. In the calculation, the one-dimensional model of the OERM platform was constructed as shown in Fig. 2(a). The platform comprised a bottom and cover glass of 1 mm thickness with 1.05 W/(Km) thermal conductivity, a 1-μm-thick a-Si:H layer with 1.8 W/(Km) thermal conductivity, and a 30-μm-thick hexadecane layer with 0.313 W/(Km) thermal conductivity.[20] The thicknesses of the gold and ITO layers were 100 and 200 nm, respectively; the heat transfer effects on these layers were relatively small and thus neglected. The platform was placed on a cooler (15 °C), and the model was cooled down to an initial temperature of 15 °C. The cover glass interacted with ambient air (25 °C), which was modeled with the heat transfer coefficient $h = 5$ W/(Km^2). In this calculation, we assumed that hexadecane melts completely at 18 °C and freezes completely at 16 °C. The generated Joule heat Q in the a-Si:H layer was calculated from the following equation based on the relationship between the applied voltage V and generated current I, which was obtained experimentally before the calculation

$$Q = V \times I \times t. \quad (3)$$

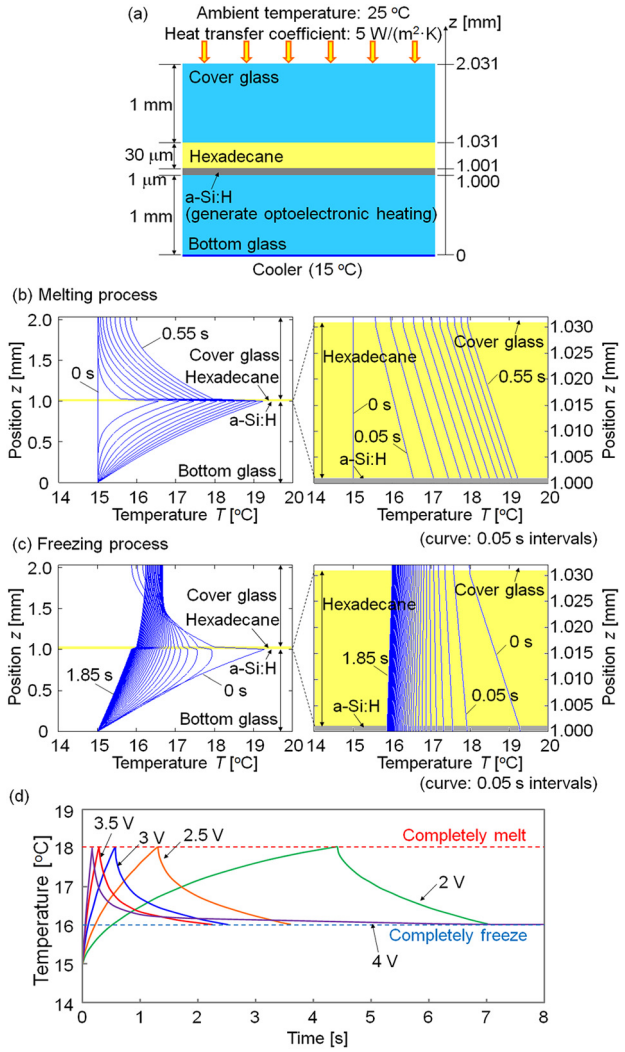

FIG. 2. Simulation results of time response during heating and cooling of hexadecane: (a) modeling of OERM platform for temperature calculation; temperature change (b) during heating and (c) during cooling with an applied bias voltage of 3.0 V; (d) 1 cycle time for melting–freezing hexadecane in the OERM at each bias voltage from 2 V to 4 V.

Figure 2(b) shows the time response of the melting process of hexadecane with optoelectronic heat when a 3.0 V bias voltage was applied to the OERM. The 3.0 V bias voltage corresponds to the generation of 1.194×10^{10} W/m^3 optoelectronic heating in the a-Si:H layer. The temperature change from the

initial temperature (15 °C) is displayed in 50-ms intervals. The temperature of hexadecane reached the melting point (18 °C) after 0.56 s from the beginning of heating.

Figure 2(c) shows the temperature distribution when the projected light was turned off. In the OERM, a small current was also generated through the a-Si:H layer, which is the dark current, even though the projected image was off.[19] The generated Joule heat by the dark current was 3.545×10^8 W/m^3 when the bias voltage was 3.0 V. In this calculation, the hexadecane was assumed to freeze when the temperature at the upper edge of the hexadecane falls below 16 °C. From the calculation results, the hexadecane temperature reached below 16 °C 1.89 s after the start of cooling when the bias voltage was 3.0 V.

The period of the melting–freezing cycle as a function of the bias voltage was investigated. The temperature at the upper edge of hexadecane ($z = 1.031$ mm) is indicated in Fig. 2(d). The melting time became shorter when the bias voltage was increased, and the melting time became less than 1 s when the bias voltage was more than 3 V. The low bias voltage took much longer to melt the hexadecane; consequently, more heat was transferred to the cover glass by the generated heat from the a-Si:H layer, and much more heat from the ambient air transferred to the cover glass. Consequently, the freezing time to cool down the heated cover glass became longer at low bias voltages. On the other hand, increasing the bias voltage caused the dark current to increase exponentially. The dark current was 5 mA at a bias voltage of 4.0 V; thus, it was not negligible.[19] Therefore, an excessively high bias voltage increases the freezing time; the hexadecane temperature did not return to below 16 °C when 4.0 V was applied. Hence, the freezing time has a minimum value. The calculation results showed that the bias voltage should be around 3.5 V to achieve the shortest operation time, which is the sum of the melting and freezing times. The melting–freezing cycle took 2.3 s when 3.5 V was applied to the OERM.

Figure 2(d) shows that the bias voltage at 3.5 V had a faster melting time than at 3 V and a shorter freezing time than at 4 V. In the experimental study, we found that 3.6 V was the best voltage to maximize the heat transfer efficiency; this was applied to the OERM as a bias voltage. The pump was demonstrated by pumping deionized (DI) water through a melting–freezing cycle (Fig. 3). The DI water from the reservoir was dyed blue with artificial coloring and placed in a reservoir at the inlet to visualize the suction effect of the pump. In the experiment, four different images were used to illustrate the pump suction. The areas enclosed by the red dashed lines of each image in Fig. 3 show the melted regions. First, two microchannels connected to the inlet and outlet, respectively, were opened by melting the frozen hexadecane (Fig. 3(a)). A large rectangle area (pumping area) was then melted (Fig. 3(b)) to generate a phase transition over a large area. The volume change generated the pumping pressure. The fluid in the melted area was then pumped out through the outlet due to the volume increase. During the freezing part of the cycle, the pump region was disconnected from the outlet and connected to the inlet (Fig. 3(c)). The light projection to the pumping area was turned off, and the hexadecane in pumping area started to freeze (Fig. 3(d)). The volume of hexadecane in the pumping area decreased, and a negative pressure was

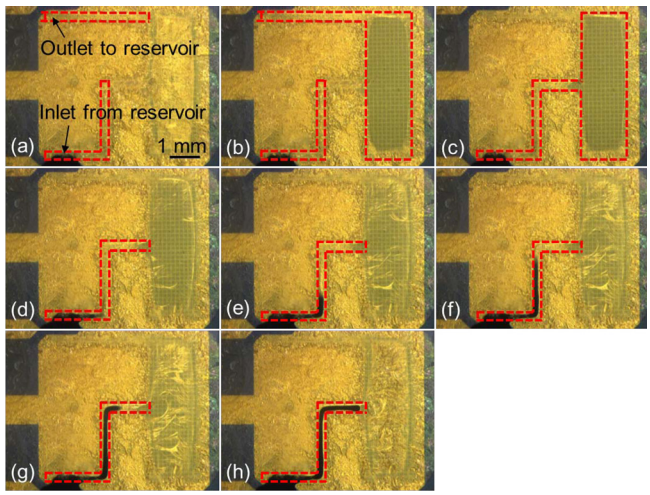

FIG. 3. Pumping of fluid: (a) open microchannels; (b) melt the pumping area connected to the outlet; (c) change the connection of pumping area from the outlet to the inlet; (d)–(h) freeze the pumping area and suck the blue-dyed water into the microchannel. The area enclosed by the red dashed lines indicates the projected light area.

generated. Consequently, blue-dyed water in the inlet was sucked through the microchannel (Figs. 3(d)–3(h)). Hence, pumping water from the inlet into the OERM platform was realized using the phase transition of hexadecane.[22] It took less than 1.5 s from the beginning (Fig. 3(d)) to the end (Fig. 3(h)) to suck the blue-dyed water into the OERM.

To evaluate the performance of the pump, the sucked volume was measured when the size of the pumping area was changed. A bias voltage of 3.6 V was applied to the OERM in each test. Figure 4(a) shows the relationship between the total melted volume of hexadecane (volume of pumping area) V_m and the generated volume of water pumped from the inlet V_s. The results show $V_s = 0.126 \times V_m$ with a correlation factor $R = 0.95$. This means that the

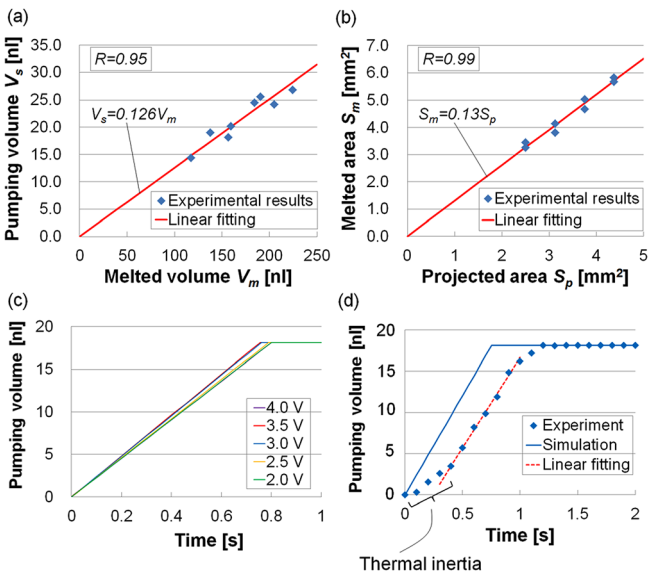

FIG. 4. Evaluation of pump when 3.6 V bias voltage was applied to the OERM: (a) relationship between the melted volume of hexadecane and pumping volume of water, (b) relationship between projected pumping area and actual melted area, (c) simulation results for pumping rate at different bias voltages, (d) time response of pumping during the phase transition from liquid to solid.

volume change was about 13% during the phase transition from liquid to solid, and the volume shrinkage was used to suck water into the microchannel. This result is close to the 11.8% volume change of hexadecane during phase transition.[18] The roughly 1% difference was attributed to the measurement error of the melted volume because the microchannel cross-section was not a perfect rectangle. Figure 4(b) shows the relationship between the projected area S_p as a pumping area and the actual melted area S_m. S_m was 1.3 times larger than S_p in the experiments due to the heat transfer on the x–y plane. The correlation factor of S_m and S_p was high ($R = 0.99$). The results indicate that the pump volume ranged from 15 nL to 27 nL. In the current setup, the light projection area for pumping can be enlarged four times. Therefore, the pumping capability can be increased to 100 nL in one cycle.

Figure 4(c) shows the simulation results of the pumping performance at different bias voltages using Eq. (2). When hexadecane finished freezing, the pumping was completed. The constant volume in the graph (Figs. 4(c) and 4(d)) represents the end of pumping. The pumping was finished after 0.8 s, and the pumping rate was constant regardless of the bias voltage. The pumping rate was related to the cooling process. The cooling depended on the heat transfer, which was constant in the system. Therefore, the pumping rate was almost the same even if the bias voltage was different. The results indicate that this type of pump is a constant rate pump. The pumping rate can be controlled by the heat transfer of the cooling system and the heat transfer rate. Hence, the pumping rate can be changed by setting the cooler temperature. Figure 4(d) shows the time response of the pumping. At 0 s, the melted pumping area started to freeze. The suction finished in about 1.2 s in the experiment. The difference in the experiment and simulation was caused by thermal inertia. The pumping rate after the thermal inertia in the experiment was 22 nL/s, which is very close to the 24 nL/s achieved in the simulation.

Different fluids (shown here by dyeing water with different colors) were pumped in the fluidic system to demonstrate the re-configurability of the pump (Fig. 5). First, blue-dyed water was sucked into the microchannel (Figs. 5(a) and 5(b)) by the same process shown in Fig. 4. Then, the inlet and outlet were switched. During the phase transition of hexadecane from solid to liquid, the line of sucked water was cut by the flow of hexadecane from the melted area, and a water droplet was formed (Figs. 5(c) and 5(d)). The red-dyed water was also sucked from the inlet (Figs. 5(e)–5(g)). Finally, the inlet and outlet were switched again (Fig. 5(h)), and both the blue- and red-dyed water were sucked and mixed in the OERM platform (Fig. 5(i)). Hence, microchannels and valves were controlled in the OERM platform simultaneously by using light patterns to switch the inlet, and different fluids were sucked by the pumps.

In conclusion, we developed a re-configurable pump that uses the volume change during phase transition and is controlled by optoelectronic heating. The pumps and valves can be generated at desired places and manipulated simultaneously by a single low-power light source. The pumping volume can be controlled within several nanoliters by the melted pump area. Hence, the current technology allows us to fabricate pumps, valves, and microfluidic channels for integration into a versatile reconfigurable microfluidic system.

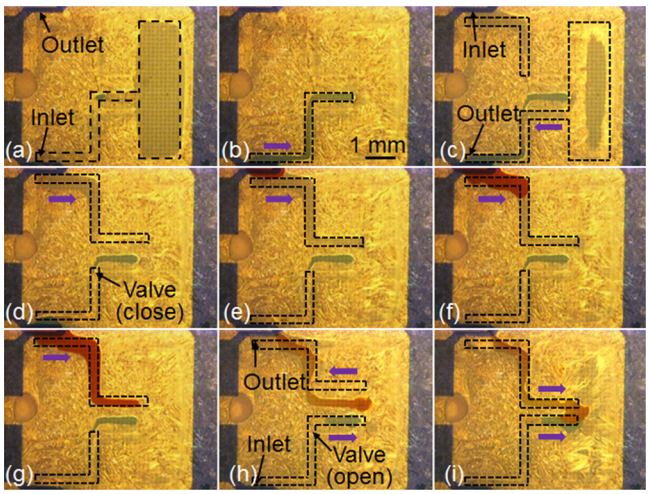

FIG. 5. Pumping differently colored water into the microchannels: (a), (b) suck blue-dyed water; (c) reverse the inlet and outlet to suck red-dyed water into another microchannel; (d)–(g) suck red–dyed water into the microchannel; (h) reverse the inlet and outlet again; (i) suck the blue- and red-dyed water simultaneously. Black dashed line indicates the edge of the lighted area.

This work was supported in part by the NSF SINAM Center (UCB/NSF 00006047), a Grant-in-Aid for JSPS Fellows (22 8644), and the Nagoya University Global COE Program (COE for Education and Research of Micro-Nano Mechatronics).

[1]G. M. Whitesides, Nature **442**, 368–373 (2006).
[2]T. M. Squires and S. R. Quake, Rev. Mod. Phys. **77**, 977–1026 (2005).
[3]Y. Wang, Z. Z. Chen, and Q. L. Li, Microchim. Acta **168**, 177–195 (2010).
[4]H. Tsutsui and C. M. Ho, Mech. Res. Commun. **36**, 92–103 (2009).
[5]J. Xie, J. Shih, Q. Lin, B. Yang, and Y. C. Tai, Lab Chip **4**, 495–501 (2004).
[6]A. Y. Fu, H. P. Chou, C. Spence, F. H. Arnold, and S. R. Quake, Anal. Chem. **74**, 2451–2457 (2002).
[7]T. Henighan, D. Giglio, A. Chen, G. Vieira, and R. Sooryakumar, Appl. Phys. Lett. **98**, 103505 (2011).
[8]S. Maruo and H. Inoue, Appl. Phys. Lett. **91**, 084101 (2007).
[9]Y. Chen, T. H. Wu, and P. Y. Chiou, Lab Chip **12**, 1771–1774 (2012).
[10]L. Liu, X. Chen, X. Niu, W. Wen, and P. Sheng, Appl. Phys. Lett. **89**, 083505 (2006).
[11]P. B. Lillehoj, F. Wei, and C. M. Ho, Lab Chip **10**, 2265–2270 (2010).
[12]M. Lian and J. Wu, Appl. Phys. Lett. **94**, 064101 (2009).
[13]R. Yokokawa, T. Saika, T. Nakayama, H. Fujita, and S. Konishi, Lab Chip **6**, 1062–1066 (2006).
[14]P. Y. Chiou, A. T. Ohta, and M. C. Wu, Nature **436**, 370–372 (2005).
[15]X. Zhu, H. Yi, and Z. Ni, Biomicrofluidic **4**, 013202 (2010).
[16]P. Y. Chiou, H. Moon, H. Toshiyoshi, C. J. Kim, and M. C. Wu, Sens. Actuators, A **104**, 222–228 (2003).
[17]D. E. Carlson and C. R. Wronski, Appl. Phys. Lett. **28**, 671–673 (1976).
[18]G. Haulot, A. J. Benahmed, and C. M. Ho, Lab Chip **12**, 5086–5092 (2012).
[19]G. Haulot and C. M. Ho, Adv. OptoElectron. **2011**, 237026.
[20]Q. Kong, J. Ma, and C. Che, Int. J. Energy Res. **33**, 513–525 (2009).
[21]H. M. Wang, J. Y. Wu, C. Y. Chen, and T. L. Chen, Biotechnol. Prog. **19**, 464–468 (2003).
[22]See supplementary material at http://dx.doi.org/10.1063/1.4824989 for the demonstration of pumping.